THE JOURNAL OF PHYSICAL CHEMISTRY C

ARTICLE

pubs.acs.org/JPCC

Interfacial Electron Transfer Dynamics in a Solar Cell Organic Dye Anchored to Semiconductor Particle and Aluminum-Doped Mesoporous Materials

Cristina Martín, Marcin Ziółek, Maria Marchena, and Abderrazzak Douhal*

Departamento de Química Física, Facultad de Ciencias Ambientales y Bioquimica and Inamol, Universidad de Castilla-La Mancha, Avda. Carlos III, S.N., 45071 Toledo, Spain

Supporting Information

ABSTRACT: We report on femto- to nanosecond emission studies of the interaction of an organic dye (TPC1) for solar cells, of (electron-donor)−(π-spacer)−(electron-acceptor) structure, with different semiconductor particles and aluminum-doped MCM-41 silicate mesoporous material, in a dichloromethane (DCM) suspension. We used ZnO, ZrO_2, and Al_2O_3 nanoparticles employed in dye-sensitized solar cells as active electron collection materials or insulating layers. Steady-state absorption and emission spectra reflect strong complex formation between TPC1 and the used materials. The femto- to nanosecond emission transients of the interfacial systems show a nonexponential behavior with an averaged half lifetime of 4, 11, and 150 ps for ZnO, ZrO_2, and Al_2O_3, respectively. For the latter, we observed the effect of the dye's concentration indicating the action of a fluorescence self-quenching mechanism. For ZnO and ZrO_2 samples, the lifetime of the complexes is determined by an electron injection rate to the conduction band and trap states of these semiconductor samples. The electron injection does not occur efficiently from the high vibrational levels of TPC1 at the S_1 state, and the subpicosecond dynamics is dominated by solvation with a time similar to that of TPC1/DCM (1.4 ps). It is in contrast with the previously observed strong emission quenching of the hot S_1 state when interacting with titania. We observed a remarkable very efficient deactivation of excited TPC1 (with half-lifetime of 1.5 ps) when interacting with Al-doped MCM-41, probably due to an electron transfer from the dye to the aluminum-doped silica framework having an acid character, and a different Al orbital configuration than that of Al_2O_3. We believe that the results presented here will enable a better understanding of the interaction of organic dyes with the surface of nanomaterials used in photovoltaics and help in exploring alternative charge-collective materials for the solar cell improvements.

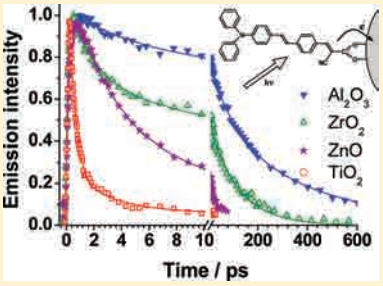

1. INTRODUCTION

Dye-sensitized solar cells (DSSCs) are one of the most encouraging photovoltaic systems.[1−3] In a typical DSSC after the light excitation of a dye, a rapid electron injection occurs from the dye to the conduction band of a titania (TiO_2) semiconductor layer, constructed as a nanoparticle film.[2,4] So far the best DSSC solar energy conversion efficiency has reached 12% with the use of Ru complex dyes.[5,6] One of the promising ways to improve the efficiency and costs of DSSCs is the use of metal-free organic dyes (instead of ruthenium compounds) and different charge collecting materials (instead of titania nanoparticles).[4]

The recently introduced triphenylamine dyes[7] have a solar light conversion efficiency comparable to that of the Ru complexes.[8] They belong to a common type of all-organic dye having (electron-donor)−(π-spacer)−(electron-acceptor) structure. We have previously measured the fast and ultrafast behavior of the most efficient dye of this family, TPC1, in different solvents,[9] as well as interacting with titania nanoparticles and nanotubes in suspensions.[10] TPC1 consists of a triphenylamine unit as an electron donor and a cyanoacrylic acid group as an electron acceptor, separated by an oligophenylenevinylene unit (Scheme 1). Although the early time photobehavior of TPC1 is quite complex due to the dominant contribution of solvation dynamics,[9] the experience from our previous studies led us to choose this dye to study its interaction with alternative semiconductor materials used in solar cells, ZnO, ZrO_2, Al_2O_3, and Al-doped mesoporous silica structures, and to compare the results with those previously obtained for TiO_2.[10] It should be noted that many recently proposed organic dyes for DSSC have electron donor−acceptor structure[4] and exhibit a large change in the dipole moment upon photoexcitation. Therefore, solvation dynamics is likely to influence their photobehavior, so the results obtained for TPC1 can be important for a large family of solar cell dyes.

The alternative electron collecting materials used in the present studies are selected for the following reasons. ZnO has a bandgap and conduction band edge similar to that of TiO_2.[2,4] The best solar cell efficiencies when using ZnO are still smaller than those when using TiO_2, but ZnO material has some potential advantages over TiO_2, like higher electron mobility

Received: April 14, 2011
Revised: October 11, 2011
Published: October 11, 2011

Scheme 1. Illustration of the TPC1 Interaction with the Used Semiconductor Particle Material (TiO_2, ZrO_2, ZnO, and Al_2O_3) and with Al-Doped MCM-41

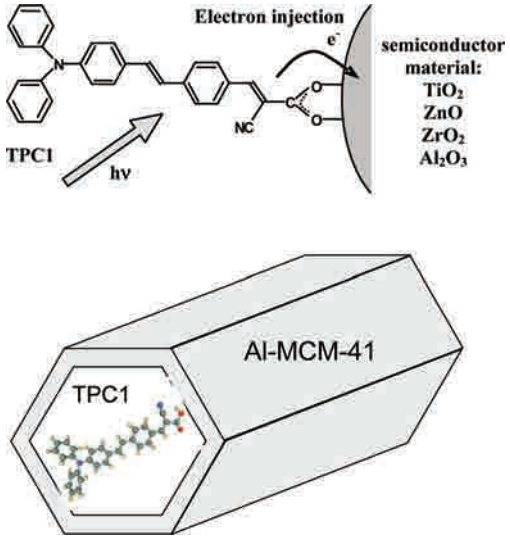

and relative ease of synthesizing highly crystalline ZnO with different morphologies (nanowires, nanotubes, nanosheets).[4,11] On the other hand, ZrO_2 and Al_2O_3 materials have a much higher position of the conduction band edge than TiO_2 and ZnO. This should prevent direct electron injection into this band from the photoexcited states of most of the dyes for solar cells. Therefore, these metal oxides (ZrO_2 and Al_2O_3) have been proposed as blocking layers deposited on titania nanoparticles to retard interfacial recombination losses, and therefore, it may improve solar cell efficiency.[12,13] However, some studies report on electron injection from the dyes to the traps states of these metal oxides: slow (1 ns) electron injection for Al_2O_3[14] and vary fast (<100 fs) for ZrO_2.[15,16] Therefore, it is important to check how these materials will interact with the TPC1 family of dyes.

Finally, one of the interesting ways to improve the dye attachment to the charge-collecting material is the use of zeolites and mesoporous hexagonal structures (MCM-41 type). The surface area of MCM-41 can reach 1000 m^2/g, which is about 20 times more than that of standard nanoparticle film. It has been shown for prototype solar cells made of Ru complexes and Ti-doped zeolites or MCM-41 that, although the total photocurrent is still low, the specific current density per titania atoms can be comparable to that of standard titania nanoparticles.[17,18] Very recently, we have studied the photobehavior of TPC1 encapsulated in specially synthesized Ti-doped MCM-41 and observed a fast electron injection.[19] Now we choose a commercially available Al-doped MCM-41 material to examine the effect of doping with a different metal which, when used as oxide (Al_2O_3), prevents from the electron injection process.

The used samples (TPC1 interacting with ZnO, ZrO_2, and Al_2O_3 nanoparticles, Al_2O_3 microparticles, and Al-doped MCM-41 powder in a dichloromethane suspension) have been studied by means of stationary absorption and emission spectroscopy and time-resolved emission spectroscopy in the temporal range from 50 fs to several nanoseconds. We observed an average fluorescence lifetime that changes from 4 to 150 ps depending on the anchoring material. The result is explained in terms of electron injection to the conduction band and trap states of the semiconductor. Interestingly, for the Al-doped MCM-41 electron-accepting material, the injection is different than that in the Al_2O_3 particle due to different Al configuration, in which the orbitals are different. The present study brings new insight into a better understanding of the photobehavior of organic dyes like the TPC1 family, when interacting with semiconductor materials for solar cell improvement and for the first time within an Al-doped silica-based mesoporous structure.

2. EXPERIMENTAL SECTION

TPC1 dye was synthesized and purified as previously described.[7] Dichloromethane (DCM, anhydrous spectral, 99.9%, Aldrich) was used as received. Semiconductor nanopowders, ZnO (particle diameter d < 100 nm), ZrO_2 (d < 100 nm), and Al_2O_3 (d < 50 nm), as well as Al_2O_3 powder (particle size: ~0.1 mm), were bought from Sigma-Aldrich. They were used after consecutive washing with *n*-hexane, tetrahydrofuran, and DCM. Aluminum-doped silicate mesoporous material (Al-MCM41, $(SiO_2)_{0.9875}(Al_2O_3)_{0.0125}$), MCM-41 type, BET area: 970 m^2/g, 2.7 nm average pore diameter) was also purchased from Sigma-Aldrich, and we reconfirmed their mesoporous structures using isothermal nitrogen adsorption and powder X-ray diffraction techniques.

All materials were dried overnight at 200 °C (to remove water) before adsorption of TPC1. Then, 100 mg of the nanopowders was added to 20 mL of TPC1/DCM solution ($c = 1.3 \times 10^{-5}$ M), ultrasonicated for half an hour, and stirred for one day at room temperature. After that, the samples were washed 3 times by centrifugation with fresh DCM. For Al_2O_3 powder (microparticles), two samples with different concentration of TPC1 per Al atom were used with 20 mL of TPC1/DCM solution (2.9×10^{-5} M) per 10 mg and 50 mg of material for the concentrated and diluted sample, respectively. For Al-MCM41 samples, three concentrations were used: 20 mL of TPC1/DCM solution (0.5×10^{-5} M) per 100 mg of material (diluted sample), 20 mL of TPC1/DCM (1.3×10^{-5} M) per 100 mg of material (normal one), and 20 mL of TPC1/DCM (4.0×10^{-5} M) per 50 mg of material (concentrated one), resulting in a total 16 times difference in TPC1 content per Al atom between the diluted and the concentrated sample.

The steady-state fluorescence and absorption spectra were measured using FluoroMax-4 (Jobin-Yvone) and JASCO V-670, respectively. The absorption spectrometer is equipped with a 60 mm integrating sphere ISN-723 allowing the studies in scattering suspension (diffuse transmittance spectra). For the diffuse transmittance, the Kubelka−Munk remittance function is used: $F(R) = (1 - R)^2/2R$, where R is the diffuse reflectance intensity from the sample. FT-IR spectra were measured using an FT-IR Perkin-Elmer spectrophotometer (model "Spectrum One") in the range 4000−240 cm^{-1}. The samples were measured diluted with KBr in a pellet and as a powder. The picosecond (ps) emission decays were measured using a time-correlated single-photon counting (TCSPC) system.[20] The sample was excited by 40 ps pulsed laser diodes centered at 433 nm (<5 mW, 40 MHz repetition rate). The emission signal was collected at the magic angle in a 25 ns window, and the instrument response function (IRF) was typically 60−90 ps. The decays were deconvoluted and fitted to multiexponential function using the FLUOFIT package allowing single and global fits. The quality of the fits was checked by examining the residual distribution and the χ^2 value.

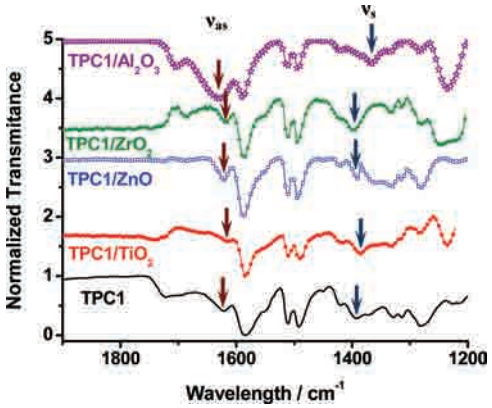

Figure 1. FTIR spectra of TPC1 interacting with different metal oxides. The positions of the asymmetric (ν_{as}) and symmetric stretching (ν_s) modes of the carboxylate unit are indicated by arrows.

Table 1. Asymmetric (ν_{as}) and Symmetric Stretching (ν_s) Modes of the Carboxylate (COO−) Unit and the Difference between Them ($\Delta\nu$) for TPC1 Interacting with Different Metal Oxides Obtained from FTIR Spectra (Figure 1)

sample	ν_{as}/cm^{-1}	ν_s/cm^{-1}	$\Delta\nu/cm^{-1}$
TPC1	1621	1392	229
TPC1/TiO_2	1617	1385	232
TPC1/ZnO	1621	1391	230
TPC1/ZrO_2	1617	1398	219
TPC1/Al_2O_3	1627	1367	260

Femtosecond (fs) emission transients have been collected using a fluorescence up-conversion technique. The system consists of a femtosecond Ti:sapphire oscillator Mai Tai HP (Spectra Physics) and coupled to second harmonic generation and up-conversion setups.[21] The oscillator pulses (90 fs, 2.5 W, 80 MHz) were centered at 840 nm and doubled in an optical setup through a 0.5 mm BBO crystal to generate a pumping beam at 420 nm (∼0.1 nJ). The polarization of the latter was set to magic angle in respect to the fundamental beam. The sample has been placed in a 1 mm thick rotating cell. The fluorescence was focused with reflective optics into a 1 mm BBO crystal and gated with the fundamental femtosecond beam. The IRF of the apparatus (measured as a Raman signal of pure solvent) was 170 fs (fwhm). To analyze the decays, a multiexponential function convoluted with the IRF was used to fit the experimental transients. All the up-conversion measurements were performed in the 200 ps time window.

3. RESULTS AND DISCUSSION

3.1. Stationary Absorption and Emission Studies. FT-IR measurements were used to establish the connection between TPC1 and different metal oxides. As was shown before, the difference between the carboxylate asymmetric ν_{as} (COO−) and symmetric bands ν_s (COO−) can be used to distinguish between bidentate and unidentate coordination.[7] Figure 1 presents the results of FT-IR studies of TPC1 alone and interacting with TiO_2, ZnO, ZrO_2, and Al_2O_3. Table 2 shows the calculated differences between the COO− asymmetric and symmetric vibrations, $\Delta\nu = \nu_{as} - \nu_s$. Previously, for TPC1 interacting with titania, the obtained values of $\Delta\nu \approx 230\ cm^{-1}$ were interpreted as the bidentate bridging mode.[7] In our case, all the samples except TPC1/Al_2O_3 have similar values of $\Delta\nu$ (Table 1). This means that for TPC1/TiO_2, TPC1/ZnO, and TPC1/ZrO_2 a similar complex is formed by bidentate bridging of the carboxylate unit of TPC1 with metal atoms on the semiconductor surface, as shown in Scheme 1. On the contrary, for TPC1/Al_2O_3 the $\Delta\nu$ value is much larger (260 cm^{-1}), and this suggests the contribution of an unidentated complex.[7]

Figure 2 shows representative stationary UV−visible absorption (diffuse) and emission spectra of TPC1 interacting with different semiconductors in DCM suspension, together with the reference spectra of the free dye in DCM. The intensity maxima of both absorption and emission bands of TPC1/Al_2O_3 shift

Table 2. Fluorescence Lifetimes (τ_i) and Their Fractional Amplitudes (A_i, Normalized to 100%) of Emission Decays of TPC1 Interacting with the Indicated Material in DCM Suspension[a]

sample	τ_1/ps (A_1/%)	τ_2/ps (A_2/%)	τ_3/ps (A_3/%)	τ_4/ns (A_4/%)
free dye	-	-	800 (96)	2.5 (4)
Al_2O_3 microparticles	-	210 (62)	650 (37)	2.6 (1)
Al_2O_3 nanoparticles	15 (50)	290(30)	840 (20)	2.3 (1)
ZrO_2	15 (85)	160 (12)	460 (3)	2.7 (<1)
ZnO	15 (100)	-	-	2.9 (<1)
Al-MCM-41	15 (51)	90 (21)	800 (27)	2.5 (1)

[a] The excitation was at 433 nm and the emission at 700 nm.

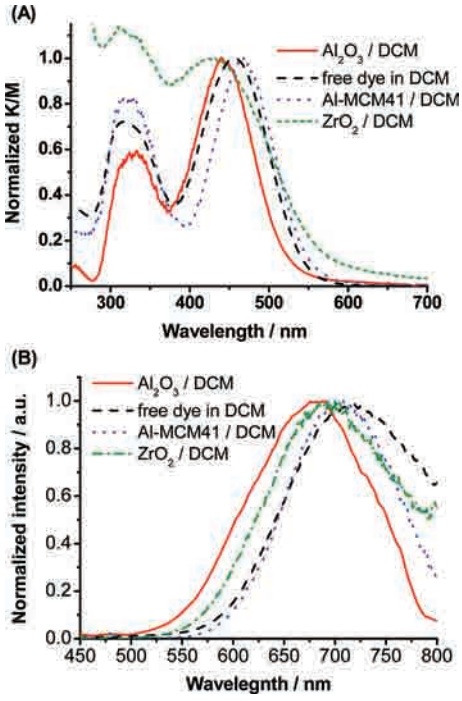

Figure 2. Steady-state UV−visible diffuse absorption (A) and emission (B, excitation at 420 nm) of TPC1 interacting with different studied nanostructures in dichloromethane (DCM). The absorption spectra of TPC1/ZrO_2 in (A) contain a significant contribution of the baseline (which intensity increases with shorter wavelength) originating probably from the trap states of ZrO_2.

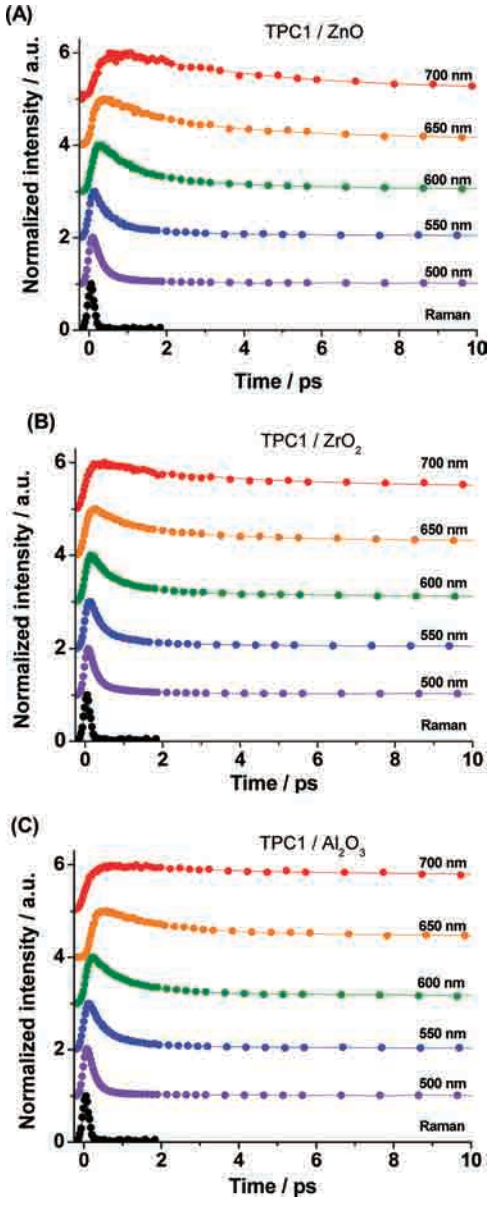

Figure 3. Femtosecond emission transients of (A) TPC1/ZnO, (B) TPC1/ZrO_2, and (C) TPC1/Al_2O_3 in DCM observed at the indicated wavelengths and upon excitation at 420 nm. The solid lines are from the best fit (see Table 3 B). The measured solvent Raman emission at 480 nm shows the IRF of the setup (fwhm = 170 fs).

slightly to the blue side by about 700 cm^{-1} with respect to those of TPC1/DCM (absorption, from 456 to 442 nm; emission, from 715 to 680 nm). The spectra (not shown) are similar for alumina nanoparticles and microparticles. The corresponding maxima of TPC1/ZrO_2 are not significantly different from those of TPC1/Al_2O_3 (Figure 2). For the TPC1/ZnO sample, it was not possible to reliably measure the stationary spectra. In the absorption measurements, the influence of the baseline originating probably from the absorption of trap states of ZnO was much higher than the absorption signal of the dye, while in the emission measurements the fluorescence signal was too low due to the much shorter lifetime of the interacting TPC1 than in other samples (see below). However, we can assume that the stationary spectra of TPC1/ZnO are similar to those of other

Table 3. Values of the Time Constants (τ_i) and Their Fractional Amplitudes (A_i, Normalized to 100%) of TPC1 Interacting with (A) ZrO_2 and (B) ZnO in DCM and Obtained from a Two- Or a Three-Exponential Function, Used to Fit the Femtosecond-Transient Emission (Convoluted With an IRF of 170 fs) at the Indicated Emission Wavelengths[a]

(A)				
λ/nm	τ_1/ps (A_1/%)	τ_2/ps (A_2/%)	τ_3/ps (A_3/%)	τ_4/ps (A_4/%)
500	-	0.17 (87)	0.90 (11)	44(2)
550	-	0.33 (86)	2.6 (11)	200 (3)
600	0.06 (−100)	0.57 (83)	8 (11)	180 (6)
650	0.10 (−100)	0.88 (60)	9 (20)	180 (20)
700	0.15 (−100)	1.4 (32)	6.7 (23)	120 (44)
(B)				
λ/nm	τ_1/ps (A_1/%)	τ_2/ps (A_2/%)	τ_3/ps (A_3/%)	τ_4/ps[b] (A_4/%)
500	-	0.22 (91)	1.4 (8)	200 (1)
550	-	0.39 (81)	2.2 (15)	200 (4)
600	0.09 (−100)	0.80 (79)	5.2 (20)	200 (1)
650	0.12 (−100)	1.5 (62)	8.1 (34)	200 (4)
700	0.26 (−100)	3.1 (63)	12 (31)	200 (6)

[a] A negative value of A_i indicates a rising component in the emission signal. [b] Fixed value in the fit.

semiconductors. The shift in the absorption and emission spectra is probably due to the anchoring effect of the dye to the semiconductor surface, which modifies HOMO and LUMO orbitals of the formed complex (with respect to those of the free dye).

Next, we report and discuss results obtained for TPC1 interacting with alumina in the Al-doped mesoporous silica framework of MCM-41 type (Al-MCM41) and also in DCM suspension. As Figure 2A shows, the absorption band of such an inclusion complex is shifted to the red by about 650 cm^{-1} with respect to that of TPC1/DCM (from 456 to 460 nm), in contrast to the blue shift of TPC1/Al_2O_3. There is also a small red shift of the maximum intensity of emission (Figure 2B). Both caging effect (in MCM-41 structure) and the different orbital of the Al atom involved in the bonding with TPC1 dye can account for the observed differences between stationary bands of TPC1/Al_2O_3 and TPC1/Al-MCM41. In Al_2O_3, octahedral hybrid orbitals are formed, while in Al-MCM41 the framework aluminum atoms are in a tetrahedral configuration leading to bridging ≡Al(OH)Si≡ groups.

3.2. Pico- to Nanosecond Time-Resolved Emission Studies. Time-correlated single-photon counting (TCSPC) studies bring information about the decay times of the relaxed excited state at S_1 of the dye interacting with the used materials. Table 2 contains the results of multiexponential fit to the decays measured at 700 nm, close to the emission maximum. For TPC1/DCM, the obtained lifetimes, 800 ps and 2.5 ns, correspond to the neutral and anion forms, respectively.[9] For TPC1 interacting with the semiconductors in DCM, the decays are not monoexponential, but the averaged decay time is shorter than that of the TPC1/DCM sample. Among the semiconductor samples, the longest lifetime is for TPC1/Al_2O_3 (two time constants: 200−300 ps and 650−850 ps), and for TPC1/ZrO_2 we got time constants of ~15, 160, and 460 ps. For TPC1/ZnO the decay is

Table 4. Values of the Time Constants (τ_i) and Their Fractional Amplitudes (A_i, Normalized to 100%) of TPC1 Interacting with (A) Al_2O_3 and (B) Al-Doped MCM-41 in DCM and Obtained from a Two- Or a Three-Exponential Function, Used to Fit the Femtosecond Transient Emission (Convoluted with an IRF of 170 fs) at the Indicated Emission Wavelengths[a]

(A)				
λ/nm	τ_1/ps (A_1/%)	τ_2/ps (A_2/%)	τ_3/ps (A_3/%)	τ_4/ps (A_4/%)
500	-	0.17 (91)	1.3 (4)	120 (<1)
550	-	0.41 (60)	2.1 (8)	200 (2)
600	0.05 (−100)	0.82 (80)	14 (10)	520 (9)
650	0.11 (−59)	1.6 (28)	53 (8)	520 (16)
700	0.20 (−86)	3.1 (16)	70 (14)	490 (52)
(B)				
λ/nm	τ_1/ps (A_1/%)	τ_2/ps (A_2/%)	τ_3/ps (A_3/%)	τ_4/ps[b] (A_4/%)
500	-	0.08 (94)	1.1 (4)	90 (2)
550	-	0.12 (88)	0.74 (10)	90 (2)
600	-	0.14 (73)	0.75 (26)	90 (1)
650	-	0.49 (81)	3.2 (14)	90 (5)
700	-	0.98 (69)	8.7 (17)	90 (14)

[a] A negative value of A_i indicates a rising component in the emission signal. [b] Fixed value in the fit.

shorter than the resolution of the TCSPC setup (~15 ps). A very small percent (1% or less) of the contribution of a 2.5 ns component arises probably from the negligible amount of TPC1 left free in suspension, which, at such a low concentration, is mostly present in an anion form.[9] As it will be discussed later, the shortening of the lifetime for alumina material with respect to that of the free dye in DCM originates most probably from some intermolecular interactions between TPC1 molecules when they are closely packed on the surface, while further emission quenching on ZrO_2 and ZnO is due to electron injection to the semiconductor at the interfaces between both species. For TPC1/Al-MCM41, the dominant decay is below 15 ps, and the other time constants are 90 ps, 800 ps, and 2.5 ns. The large shortening of TPC1 lifetime when interacting with Al-MCM41 pores compared to that on the Al_2O_3 particle will be also explained later.

3.3. Femto- to Picosecond Time-Resolved Emission Studies of TPC1 Interacting with Semiconductor Particles. To get a deeper insight into the interactions of the dye with the semiconductors at the earliest time dynamics, we performed femtosecond up-conversion emission studies. We excited at 420 nm and gated the emission from 500 to 700 nm (each 50 nm). Figure 3 and Figure S1 (in the Supporting Information, SI) show illustrative emission transients at different gating wavelengths. Tables 3 and 4 give the results of the multiexponential fits. As we reported previously, the ultrafast transients of the free dye in polar solvents (both TPC1 normal and anion forms) are dominated by solvation dynamics (1.4 ps in DCM), due to a large change in the dipole moment of the dye upon excitation to S_1.[9] The solvation is manifested as a dynamic red shift (by about 5500 cm^{-1}) of the emission spectrum band with time, being responsible for the fast decays in the blue part and fast rises in the red part of the spectrum. The longer decays in the red part are

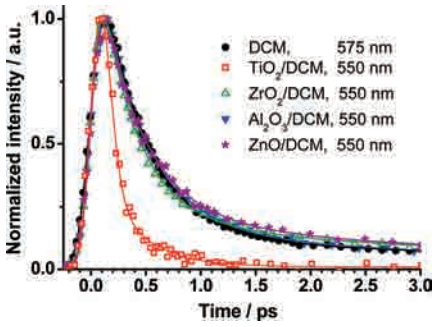

Figure 4. Comparison of femtosecond emission transients of the indicated samples (inset) gated at 550 nm and upon excitation at 420 nm. The solid lines are from the best fits (see Tables 3 and 4). The results obtained previously for TPC1 in DCM at 575 nm and TPC1−TiO_2 at 550 nm are added for comparison.[9,10]

due to the decay of the relaxed charge transfer (CT) state with the time constant of 800 ps.[9]

The present experiments show that the same trend is observed for TPC1 interacting with the semiconductors studied here. As we see in Tables 3 and 4, the transients measured at the very blue side of the emission band (500 and 550 nm) are very similar for Al_2O_3, ZrO_2, and ZnO samples. Figure 4 illustrates an example of the transients measured at 550 nm for the three samples and compared to TPC1/DCM at 575 nm (the different wavelength is chosen to account for the 700 cm^{-1} shift in the emission band). The transients are almost identical, and this has two main implications. First, the similarity between TPC1/DCM and TPC1/Al_2O_3 transients (with no possibility of electron injection) indicates that there is no difference in the solvation (and vibrational relaxation) dynamics between the free dyes and those adsorbed on the semiconductor surface (when suspended in DCM). Second, the similar transients observed for TPC1/ZrO_2 and TPC1/ZnO suggest the absence of an efficient electron injection from the vibrationally hot excited states of TPC1 at S_1 to the acceptor "states" in the semiconductor. This is in contrast with the results of the interaction of TPC1 with titania particles in DCM and acetonitrile suspensions that we recently measured.[10] The transient of TPC1/TiO_2 in DCM at 550 nm is also added for comparison in Figure 4, and it is clear that it is much faster than those for the other samples. The observed additional quenching using TiO_2 nanoparticles is due to electron injection from the high vibrational levels of the S_1 state. It is worth noting that the absence of this process in the ZnO semiconductor, having the same position of the conduction band as TiO_2, implies that the electron injection rate in ZnO is much smaller than that in TiO_2 and cannot compete with fast vibrational relaxation and solvation dynamics.

The differences in the fluorescence dynamics of TPC1 when interacting with Al_2O_3, ZrO_2, and ZnO particles in DCM are examined at 600 nm and longer gating wavelengths, when the lifetime of the relaxed S_1 state of the dye starts to strongly contribute to the emission transients (Tables 3 and 4). The longest gating wavelength available in our experiment (700 nm) can be considered as the most representative one to measure the lifetime of the relaxed state since the influence of vibrational relaxation is minimized. Figure 5 presents a comparison of the emission transients using Al_2O_3, ZrO_2, and ZnO particles, together with those of TPC1/TiO_2[10] and TPC1/DCM,[9] all gated at 700 nm. In line with the TCSPC results (section 3.2),

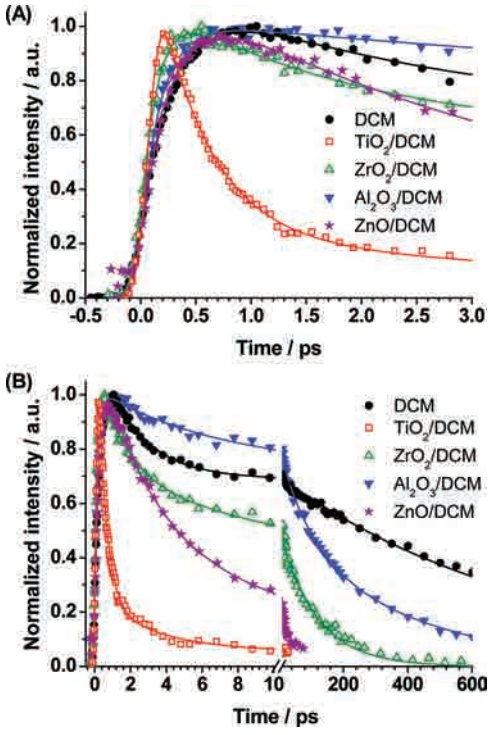

Figure 5. Comparison of femtosecond emission transients of the indicated samples (inset) gated at 700 nm and upon excitation at 420 nm. The solid lines are from the best fits (see Tables 3 and 4). The results obtained previously for TPC1 in DCM and TPC1−TiO_2 at 700 nm are added for comparison.[9,10]

among the three studied semiconductors the shortest lifetime is observed for the ZnO sample (time constants 3.1 and 12 ps), the medium one for ZrO_2 (times 1.4, 6.7, and 120 ps), and the longest for Al_2O_3 (times 3.1, 70, and 490 ps). As for the small offset observed for TPC1/ZnO (time constant >200 ps), it is probably from a weak contribution of free dye molecules in solution, as we previously explained for TPC1/TiO_2.[10] When the emission is gated at 700 nm, TPC1 solvation is reflected as a rise time in the gated signal,[9] and in agreement with the conclusions presented above, the similar rise times observed for TPC1 on Al_2O_3 (0.20 ps), ZrO_2 (0.15 ps), ZnO (0.26 ps), and free TPC1 (0.33 ps) in DCM (Figure 5A) confirm a similar (in time domain) solvation dynamics in the four samples. For TPC1/TiO_2 the quenching due to electron injection is too fast to observe the rise time.

At this point, some limitations in the observation of electron injection dynamics (from TCP1 to the semiconductors nanoparticles) should be considered. They are due to the fact that the time-resolved emission studies applied in this study probe only the decay of the TPC1 excited state, not directly the presence of electrons in the conduction band. Therefore, a very fast electron injection from the vibronically hot excited state[22] might not be observed if it is faster than the temporal resolution of the setup (<50 fs). Second, some small contribution of the electron injection that occurs in the subpicosecond regime might be hidden under the dominant signal of the solvation dynamics taking place on a similar time scale. However, we estimate the latter contribution in TPC1/ZnO, TPC1/ZrO_2, and TPC1/Al_2O_3 as not higher than 10% of the total amplitude of the fluorescence decay—otherwise a clear change in the

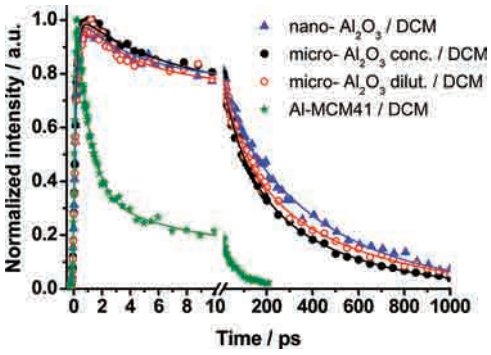

Figure 6. Comparison of 700 nm femtosecond emission transients of a DCM suspension containing TPC1 interacting with alumina particles of different size and at different concentrations of the dye and with Al-doped material. The solid lines are from the best fit (Table S2, SI). The preparation conditions of TPC1/Al_2O_3 nanoparticles (nano-Al_2O_3), diluted TPC1/Al_2O_3 microparticles (micro-Al_2O_3 dilut.), and concentrated TPC1/Al_2O_3 microparticles (micro-Al_2O_3 conc.) are given in the Experimental section.

kinetics shape should be observed, like for TPC1/TiO_2 samples (Figures 5 and 6).

Previously, we have reported on the nonexponential dynamics of electron injection in TPC1/TiO_2.[10] Such behavior has also been observed for some dye/titania systems prepared for solar cells.[23,24] The multiexponential behavior was explained using a model in which the distribution of electron injection rate constants is due to the heterogeneity in the interface contacts.[23−25] In the model, the microscopic rate of electron transfer is proportional to g, the density of acceptor states in the semiconductor, which is exponentially increasing with energy E[26]

$$g(E) = g_0 \exp[-(E - E_C)/E_0] \quad (1)$$

where E_C is the conduction band edge energy; g_0 is a constant; and E_0 describes the average trap depth with a reported value between 0.06 and 0.2 eV.[25,27] Due to the inhomogeneity in the titania sample (a nonperfect smooth surface), the relative energy of the conduction band and the excited state of the dye vary slightly due to the variance in the interface contacts. This results in an energetic shift of the exponential function of acceptor states density for different dye−titania pairs and a macroscopic distribution of electron injection rates. If we assume a Gaussian distribution of the energetic variations, the results of simulation show a very good fit to the experimental data, with the fwhm of Gaussian between $1.5E_0$ and $3.7E_0$.[23,24] Such heterogeneous behavior is more likely to be observed when the energy position of the dye at the excited state is close to or below the conduction band edge, $E \sim E_C$. Indeed, we have recently estimated that such a condition can be valid for the relaxed S_1 state of TPC1 interacting with titania in a polar suspension.[10] The position of the conduction band edge of ZnO is similar to that of TiO_2,[2,4] and those of ZrO_2 and Al_2O_3 are even higher,[12] so the above model can also be applied to explain the results of the present studies.

The easiest way to compare the multiexponential fluorescence quenching dynamics of TPC1 interacting with the used semiconductors is to take decay half-lifetimes as the measure of a mean fluorescence lifetime. These values at 700 nm are: 0.5 ps for TiO_2, 4 ps for ZnO, 11 ps for ZrO_2, and 150 ps for Al_2O_3 (Figure 5). They are shown in Scheme 2 as the averaged lifetime

Scheme 2. Relative Presentation of Energy Diagram of TPC1 S_0 and S_1 States and of the Used Semiconductor Material at Their Valence (VB) and Conduction (CB) Bands[a]

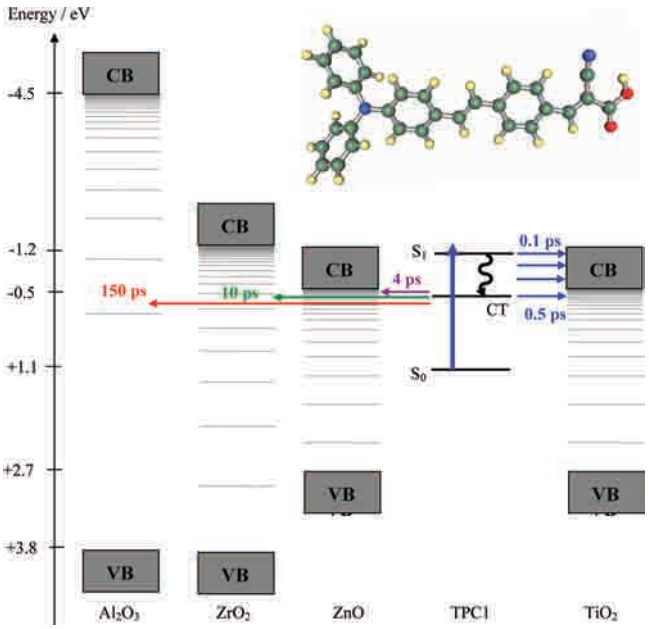

[a] The scheme gives the value of the averaged fluorescence time constants resulting in the interaction of TPC1 with the semiconductors and electron injection.

of each system, together with the position of ground and excited state oxidation potentials of TPC1 and the valence and conduction band potentials of the semiconductors studied here.[2,12] The difference between TiO_2 and ZnO can be explained in terms of the differences in the conduction band electronic structures of both semiconductors. It has been observed for other systems that the electron injection rate is faster in TiO_2 than in ZnO due to the higher density of states formed by d orbitals of Ti^{4+} than those formed by s and p orbitals of Zn^{2+}.[28] This orbital property not only explains the longer lifetime of TPC1/ZnO but also reflects the lack of efficient electron injection from the hot excited state in TPC1/ZnO as we previously noticed. For the ZrO_2 sample, the reason of the lower electron injection rate is most probably the value of E_C, which is 0.7 eV higher than for TiO_2.[12,15] This implies that the electrons can only be injected into the trap states of ZrO_2 of much lower density than those of TiO_2. As mentioned in the Introduction, such electron injection to the trap states has been frequently observed.[15,16] Assuming the same value of the g_0 parameter for both ZrO_2 and TiO_2 particles, eq 1 predicts 33 times lower density of electron acceptor states in ZrO_2 than in TiO_2 (for the same energy level E). This value is in reasonable agreement with the ratio of the half-lifetimes observed in both semiconductors (11 ps in ZrO_2 and 0.5 ps in TiO_2, resulting in the ratio of 22). On the contrary, Al_2O_3 has an E_C value about 4 eV higher than that of TiO_2,[12] and eq 1 predicts more than 8 orders of magnitude lower density of electron-accepting states. Therefore, the contribution of the electron injection process in the fluorescence quenching of TPC1/Al_2O_3 can be neglected, in line with the reports using other dyes.[29,30]

On the other hand, it has also been shown that nonexponential electron injection kinetics in heterogeneous systems can be described, empirically, by the stretched exponential function

$$f(t) = A \exp[(-t/\tau_S)^{\alpha}] \quad (2)$$

where τ_S is a characteristic (mean) time of the decay and α is the heterogeneity (dispersion), with α values typically between 0.3 and 0.65[24,31] (mathematically this parameter can have values between 0 and 1; $\alpha = 1$ is for monoexponential decay, and a smaller value indicates more dispersive kinetics). Smaller values of α indicate a broader Gaussian distribution of the energetic variations, while τ_S is proportional to the injection rate in the center of Gaussian distribution. In our case, when the stretched exponential function was applied to the emission signal at 700 nm, we obtained α ranging from 0.37 to 0.70 and τ_S equal to: 0.7 ps for TiO_2, 5.6 ps for ZnO, 21 ps for ZrO_2, and 260 ps for Al_2O_3 (Table S1B, SI). The stretched exponential function could also be fitted to the emission transients measured in the TCSPC experiment for ZrO_2 and Al_2O_3 samples, giving times of 80 and 300 ps, respectively (Table S1A, SI). Slightly longer values of τ_S from TCSPC experiments than up-conversion ones are due to the fact that the fast kinetics (<15 ps) are not resolved in the former one. The two parameters of stretched exponential function (α and τ_S) fitted to the experimental signals should be considered as a more precise description of the fluorescence decay than the previously derived half-lifetimes.

As we concluded before, the contribution of interfacial electron injection in alumina samples should be neglected. However, the kinetics are multiexponential and can be fitted using a stretched exponential function, like for other semiconductors in which the electron injection is the main deactivation channel of the relaxed S_1 state of the dye. Therefore, most probably, the dyes' self-quenching processes are responsible for the deactivation of TPC1 on alumina. The typical mechanisms responsible for the shortening of the excited state lifetime might be singlet−singlet annihilation[32,33] or energy homotransfer between the excited molecules and aggregates.[34] Alternatively, intermolecular electron transfer between dye dimers yielding to radical pair formation has been also proposed for some systems to explain the emission decay.[35] The intermolecular resonance energy-transfer process usually results in a nonexponential dynamics and can be modeled also by a stretched exponential function.[36−38] Thus, to get more insight into the photobehavior of TPC1 on an alumina particle in DCM, we compared the results measured using different sizes of alumina particles (nano- and microparticles) and at different concentrations of TPC1 per Al atom. The absorption and emission spectra are the same for all the used samples (not shown). Figure 6 summarizes the most representative results of the 700 nm emission transients up to 1 ns, while Table S2 (SI) gives the results of the multiexponential fits. The emission transient does not depend on the size of the Al_2O_3 particle. The small differences can be largely explained by different dye concentrations. The stretched exponential fit results shown in Table S1 (SI) reveal the longest decay for Al_2O_3 nanoparticles (τ_S = 300 ps and τ_S = 260 ps in TCSPC and up-conversion experiments, respectively) and the shortest for concentrated Al_2O_3 microparticles (τ_S = 230 ps and τ_S = 170 ps in TCSPC and up-conversion experiments, respectively). These two samples have 22 times different concentrations of TPC1 per Al atom. Therefore, these results confirm the impact of the dye concentration on the observed transients on alumina. However, the similar values of α indicate the same stretched-exponential character of the emission transients, irrespective

of the concentration. Therefore, either all the concentrations investigated in our experiment correspond to strong self-quenching regime or there are also other processes responsible for the dispersion in the fluorescence lifetimes on alumina.

3.4. Femto- to Picosecond Time-Resolved Emission Studies of TPC1 Interacting with Al-Doped MCM-41. Finally, we report a very interesting time-resolved emission result obtained for TPC1 interacting with Al-MCM41. The most striking difference between TPC1/Al_2O_3 and TPC1/Al-MCM41 is a very efficient emission quenching observed in the latter sample. As we can see in Figure 6, the half-lifetime of the TPC1/Al-MCM41 fluorescence gated at 700 nm is 1.5 ps, which is not only much shorter than that of TPC1/Al_2O_3 (150 ps) but also shorter than those for the other two semiconductors studied here in which electron injection takes place (ZnO and ZrO_2). Table 4B shows the results of the multiexponential fits of the transients at different gating wavelengths, while Figure S2 (in SI) exhibits the corresponding emission transients for TPC1/Al-MCM41. Clearly, the fluorescence decays of TPC1/Al-MCM41 are faster than those of ZnO, ZrO_2, and Al_2O_3 for all wavelengths (from 500 to 700 nm), and no rise components are observed for Al-MCM41 in the range 600−700 nm. This behavior indicates that the process responsible for the fluorescence quenching is already effecting the transients at high vibrational levels of the S_1 state, like when TPC1 interacts with titania nanoparticles.[10]

In Al-MCM41 material the presence of Al atoms replacing isomorphically Si ones in the regular MCM-41 introduces a Brönsted acidity which is due to the presence of bridging ≡Al(OH)Si≡ groups. Such acidity increases the electron acceptor ability of aluminosilicates, and it has been determined that the electron acceptor strength follows the order of acid strength, stronger acid sites being strong oxidizing centers.[39] The radical cations centered on the triphenylamine moiety have been observed for the molecules caged in aluminasilicate zeolites, both by spontaneous generation at the ground state[40] and after photoexcitation.[41] Moreover, for TPC1/regular MCM-41 in DCM we have observed a very stable and strong absorption band of the TPC1 cation (absorption maximum at 690 nm) generated by an electron transfer from the dye at S_0.[19] Therefore, one possibility to account for the emission quenching of TPC1 in Al-doped MCM-41 is that upon excitation an electron is photochemically transferred from TCP1 molecules that are interacting with the acid sites.

To exclude the contribution of singlet−singlet annihilation or energy transfer between TPC1 aggregates in the observed fluorescence quenching of TPC1/Al-MCM41, we analyzed the dependences of the emission transients on excitation fluence and concentration. Figure S3 (in SI) shows that the emission kinetics do not change when varying the dye content per alumina and the laser power, respectively. In our previous study of TPC1 in pure MCM-41 we have also observed that the caging effect of the nanopore (∼2.5 nm) itself cannot be responsible for the efficient fluorescence quenching.[19] Therefore, the emission quenching in TPC1/Al-MCM41 samples mainly originates from electron injection from the dye to the MCM-41 Brönsted acid sites associated with the tetrahedral Al framework. Importantly, the fast creation of the TPC1 radical cation in Al-MCM41 is reminiscent of the electron injection process in the semiconductors used for solar cells. If the photoinduced radical cation formation is stable in TPC1/Al-MCM41, and the electrons can jump between several acid sites along a reasonable distance within the mesoporous structure, the Al-doped MCM-41 material can be more explored for proposing it as a new charge-collecting material for a new generation of DSSCs. Obviously, further studies are necessary to prove this possibility.

4. CONCLUSION

In this contribution, we have studied the interactions between TPC1 and three semiconductor particles used in solar cells: ZnO, ZrO_2, and Al_2O_3. For alumina one, we also investigated the effects of the size of the material (nano- and microparticles) and the inclusion (Al doping) in MCM-41 type mesoporous molecular sieves. We observed that the initial relaxation of the vibrationally hot states at S_1 of TPC1 interacting with the three used metal oxide nanoparticles in DCM solutions takes place with the same dynamics as that of free dye in DCM, and it is dominated by solvation of the TPC1 charge transfer state in a polar environment. The fluorescence of the relaxed S_1 state decays in a nonexponential way with the half-lifetimes of 4, 11, and 150 ps for ZnO, ZrO_2, and Al_2O_3, respectively. For the first two samples, the lifetime is determined by the electron injection rate to the conduction band and trap states of the used semiconductor. Only for the alumina case, we observed the effect of the dye's concentration indicating the presence of fluorescence self-quenching. These results differ significantly from those previously reported for the same dye interacting with titania, where efficient electron injection from the hot S_1 state was found, and the half-lifetime of the relaxed S_1 state was short, 0.5 ps.[10] The slower electron injection rate to ZrO_2 than to TiO_2 is explained by a higher energetic position of the conduction band edge for the former, implying the involvement of deep trap states in the electron transfer process (Scheme 2). On the contrary, the differences between electron injection dynamics for ZnO and TiO_2 are probably due to different electronic structures and density of states in the conduction band of these semiconductors. Finally, we observed a very efficient emission quenching of TPC1 interacting with Al-doped MCM-41 material (half-lifetime 1.5 ps of the relaxed S_1 state). It is rationalized by an electron transfer route to the acid bridging Al(OH)Si groups. We believe that the efficiency of this process suggests further exploration of the Al-doped MCM-41 material for DSSC development.

■ ASSOCIATED CONTENT

Ⓢ Supporting Information. Figures S1−S3 and Tables S1−S2. This material is available free of charge via the Internet at http://pubs.acs.org.

■ AUTHOR INFORMATION

Corresponding Author

*E-mail: abderrazzak.douhal@uclm.es.

■ ACKNOWLEDGMENT

The research leading to these results has received funding from the European Community's Seventh Framework Programme (FP7/2007-2013) under grant agreement n° 235286 (NANOSOL). This work was also supported by the MICINN through projects PLE 2009-0015 and MAT2008-01609, respectively, and Consolider-Ingenio 2010 (CDS2009-00050). We thank Prof. Licheng Sun and Dr. Xichuan Yang for giving us the TPC1 dye and Laura Ramos (CSIC, Madrid) for helping in

recording the IR spectra. C.M. thanks the MEC for the PhD fellowship.

REFERENCES

(1) O'Regan, B.; Grätzel, M. *Nature* **1991**, *353*, 737–740.
(2) Grätzel, M. *Nature* **2001**, *414*, 338–344.
(3) Kamat, P. V. *J. Phys. Chem. C* **2007**, *111*, 2834–2860.
(4) Hagfeldt, A.; Boschloo, G.; Sun, L.; Kloo, L.; Pettersson, H. *Chem. Rev.* **2010**, *110*, 6595–6663.
(5) Nazeeruddin, M. K.; De Angelis, F.; Fantacci, S.; Selloni, A.; Viscardi, G.; Liska, P.; Ito, S.; Takeru, B.; Grätzel, M. *J. Am. Chem. Soc.* **2005**, *127*, 16835–16847.
(6) Yu, Q.; Wang, Y.; Yi, Z.; Zu, N.; Zhang, J.; Zhang, M.; Wang, P. *ACS Nano* **2010**, *4*, 6032–6038.
(7) Tian, H.; Yang, X.; Chen, R.; Zhang, R.; Hagfeldt, A.; Sun, L. *J. Phys. Chem. C* **2008**, *112*, 11023–11033.
(8) Hwang, S.; Lee, J. H.; Park, C.; Lee, H.; Kim, C.; Park, C.; Lee, M.-H.; Lee, W.; Park, J.; Kim, K.; Park, N.-G.; et al. *Chem. Commun.* **2007**, 4887–4889.
(9) Ziółek, M.; Yang, X.; Sun, L.; Douhal, A. *Phys. Chem. Chem. Phys.* **2010**, *12*, 8098–8107.
(10) Ziółek, M.; Tacchini, I.; Martínez, M. T.; Yang, X.; Sun, L.; Douhal, A. *Phys. Chem. Chem. Phys.* **2011**, *13*, 4032–4044.
(11) Zhang, Q.; Dandeneau, C. S.; Zhou, X.; Cao, G. *Adv. Mater.* **2009**, *21*, 4087–4108.
(12) Palomares, E.; Clifford, J. N.; Haque, S. A.; Lutz, T.; Durrant, J. R. *J. Am. Chem. Soc.* **2003**, *125*, 475–482.
(13) Kay, A.; Grätzel, M. *Chem. Mater.* **2002**, *14*, 2930–2935.
(14) Asbury, J. B.; Ellingson, R. J.; Ghosh, H. N.; Ferrere, S.; Nozik, A. J.; Lian, T. *J. Phys. Chem. B* **1999**, *103*, 3110–3119.
(15) Ramakrishna, G.; Singh, A. K.; Ghosh, H. N.; Palit, D. K. *J. Phys. Chem. B* **2004**, *108*, 4775–4783.
(16) Huber, R.; Spörlein, S.; Moser, J. E.; Grätzel, M.; Wachtveitl, J. *J. Phys. Chem. B* **2000**, *104*, 8995–9003.
(17) Atienzar, P.; Valencia, S.; Corma, A.; Garcia, H. *ChemPhysChem* **2007**, *8*, 1115–1119.
(18) Atienzar, P.; Navarro, M.; Corma, A.; Garcia, H. *ChemPhysChem* **2009**, *10*, 252–256.
(19) Ziółek, M.; Martín, C.; Navarro, M.; Garcia, H.; Douhal, A. *J. Phys. Chem. C* **2011**, *115*, 8858–8867.
(20) Organero, J. A.; Tormo, L.; Douhal, A. *Chem. Phys. Lett.* **2002**, *363*, 409–414.
(21) Gil, M.; Douhal, A. *Chem. Phys. Lett.* **2006**, *428*, 174–177.
(22) Moser, J. E.; Wolf, M.; Lenzmann, F.; Grätzel, M. *Z. Phys. Chem.* **1999**, *212*, 85–92.
(23) Haque, S. A.; Palomares, E.; Cho, B. M.; Green, A. N. M.; Hirata, N.; Klug, D. R.; Durrant, J. R. *J. Am. Chem. Soc.* **2005**, *127*, 3456–3462.
(24) Koops, S. E.; Durrant, J. R. *Inorg. Chim. Acta* **2008**, *361*, 663–670.
(25) Tachibana, Y.; Rubtsov, I. V.; Montanari, I.; Yoshihara, K.; Klug, D. R.; Durrant, J. R. *J. Photochem. Photobiol. A: Chem.* **2001**, *142*, 215–220.
(26) Frank, A. J.; Kopidakis, N.; van de Lagemaat, J. *Coord. Chem. Rev.* **2004**, *248*, 1165–1179.
(27) Tisdale, W. A.; Muntwiler, M.; Norris, D. J.; Aydil, E. S.; Zhu, X. Y. *J. Phys. Chem. C* **2008**, *112*, 14682–14692.
(28) Anderson, N. A.; Lian, T. *Annu. Rev. Phys. Chem.* **2005**, *56*, 491–519.
(29) Myllyperkiö, P.; Manzoni, C.; Polli, D.; Cerullo, G.; Korppi-Tommola, J. *J. Phys. Chem. C* **2009**, *113*, 13985–13992.
(30) Vinodgopal, K.; Hua, X.; Dahlgren, R. L.; Lappin, A. G.; Patterson, L. K.; Kamat, P. V. *J. Phys. Chem.* **1995**, *99*, 10883–10889.
(31) Koops, S. E.; O'Regan, B. C.; Barnes, P. R. F.; Durrant, J. R. *J. Am. Chem. Soc.* **2009**, *131*, 4808–4818.
(32) Billsten, H. H.; Sundström, V.; Polívka, T. *J. Phys. Chem. A* **2005**, *109*, 1521–1529.
(33) Ito, F.; Inoue, T.; Tomita, D.; Nagamura, T. *J. Phys. Chem. B* **2009**, *113*, 5458–5463.
(34) Luo, L.; Lo, C.-F.; Lin, C.-Y.; Chang, I.-J.; Diau, E. W.-G. *Phys. Chem. Chem. Phys.* **2010**, *12*, 1064–1071.
(35) Pelet, S.; Grätzel, M.; Moser, J.-E. *J. Phys. Chem. B* **2003**, *107*, 3215–3224.
(36) Förster, T. *Z. Naturforsch.* **1949**, *4a*, 321.
(37) Lutkouskaya, K.; Calzaferri, G. *J. Phys. Chem. B* **2006**, *110*, 5633–5638.
(38) Gil, M.; Ziółek, M.; Organero, J. A.; Douhal, A. *J. Phys. Chem. C* **2010**, *114*, 9554–9562.
(39) García, H.; Roth, H. D. *Chem. Rev.* **2002**, *102*, 3947–4007.
(40) García, H.; Martí, V.; Casades, I.; Fornés, V.; Roth, H. D. *Phys. Chem. Chem. Phys.* **2001**, *3*, 2955–2960.
(41) Doménech, A.; Ferrer, B.; Fornés, V.; García, H.; Leyva, A. *Tetrahedron* **2005**, *61*, 791–796.